J. Fluid Mech. (1973), *vol.* 57, *part* 3, *pp.* 603–622
Printed in Great Britain

Turbulence in a conical diffuser with fully developed flow at entry

By P. A. C. OKWUOBI AND R. S. AZAD
Department of Mechanical Engineering, The University of Manitoba, Winnipeg, Canada

(Received 14 May 1972)

An experimental study of the structure of turbulence in a conical diffuser having a total divergence angle of 8° and an area ratio of 4:1 with fully developed flow at entry is described. The research has been done for pipe entry Reynolds numbers of 152 000 and 293 000 of profiles of the mean pressure, mean velocity, turbulence intensities, correlation coefficients and the one-dimensional energy spectra, but owing to similar behaviour for these two Reynolds numbers, data are presented for a Reynolds number of 293 000.

The results show that the rate of turbulent energy production approximately reaches a maximum value at the edge of the wall layer extending to the point of maximum u_1-fluctuation. It is found that, within the layer, $\overline{u_1^2}$ varies linearly with the distance from the wall and the linear range grows with distance in the downstream direction.

The turbulent kinetic energy balance indicates that the magnitude of the energy convective diffusion due to kinetic and pressure effects is comparable with that of the energy production.

1. Introduction

The importance of the diffuser as a simple, useful, fluid-mechanical element in closed-circuit wind tunnels and in turbomachinery has been known ever since Venturi (1797) and his contemporaries tried to determine the geometry for the most efficient diffuser. Since then, a vast number of experimental and theoretical studies (e.g. Gibson 1910; Patterson 1938; Fraser 1956; Sprenger 1959; Kline, Abbott & Fox 1959; Sovran & Klomp 1967; Ackeret 1967; Cockrell & King 1967) have been devoted to the subject. The results of these investigations are summarized in Cocanower, Kline & Johnston (1965), Cockrell & King (1967) and Schlichting (1968).

The one aspect of diffuser study which until recently has received little attention is the investigation of the turbulence characteristics of the flow field. The structure of turbulent shear flow in a diffuser was probably first studied by Ruetenik & Corrsin (1955). They investigated the turbulence properties of fully developed, plane diffuser flow at a total divergence angle $\alpha = 2°$; comparison of their results with those of Laufer (1951) for parallel wall channel flow showed that there were large increases in turbulent energy and average shear levels. Previously published turbulence measurements in a conical diffuser include those

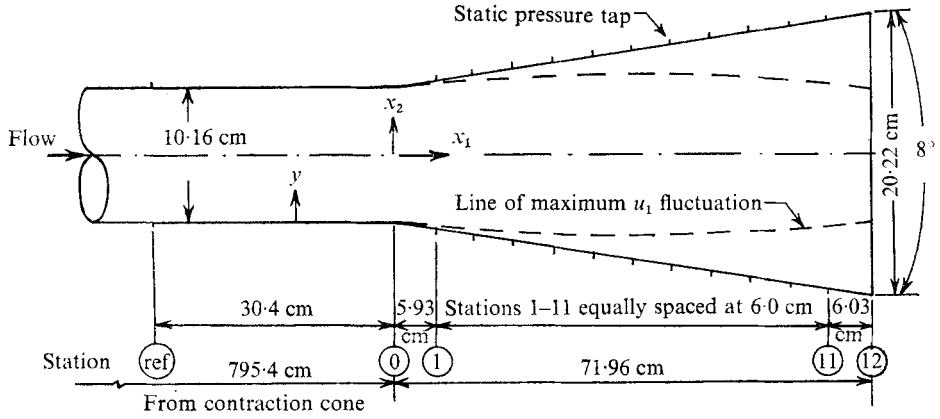

FIGURE 1. Diffuser geometry.

of Robertson & Calehuff (1957) for $\alpha = 7\frac{1}{2}°$ and Trupp *et al.* (1971) for $\alpha = 8°$. Robertson & Calehuff observed that the turbulence levels, the rates of turbulence production and dissipation were greatly in excess of similar quantities for zero-pressure-gradient boundary layers and that the longitudinal microscales of turbulence remained remarkably constant across and along the developing diffuser flow. Trupp *et al.* investigated diffuser flow with a partly developed pipe flow at entry; they found that the effect of Reynolds number (within the range tested) on the distribution of the turbulence intensities was negligible, and that the relationship between the turbulent shear stress and the turbulent kinetic energy was approximately linear as noted by Harsha & Lee (1970).

Flow through diffusers does not usually possess the simplified features of fully developed flow and it may be expected that any mathematical model of turbulence formulated with reference to the existing experimental data for symmetric equilibrium flows will be inadequate when used to predict diffuser flows in moderate to strong adverse pressure gradients. It thus appeared desirable to provide more quantitative data than has hitherto been available on the turbulence properties of conical diffuser flow. This information should also be useful as a test case for future calculation methods for predicting the distribution of mean and turbulent quantities in a diffuser.

Measurements of the turbulence quantities were to be made using the hot-wire technique; the choice of the diffuser geometry was guided by the work of Sprenger (1959) and Sovran & Klomp (1967), whose results show that the 8° conical diffuser of area ratio 4:1 possesses optimum pressure recovery characteristics.

2. Experimental equipment and procedures

2.1. *Wind tunnel and diffuser*

The low-speed open-circuit wind tunnel used in the experiment has been described by Azad & Hummel (1971). Seventy-eight diameters of straight pipe separated the contraction cone from the start of the diffuser.

The diffuser (figure 1) was machined from cast aluminum. Static pressure holes, 0·6 mm in diameter and spaced 90° apart, were inserted at each station;

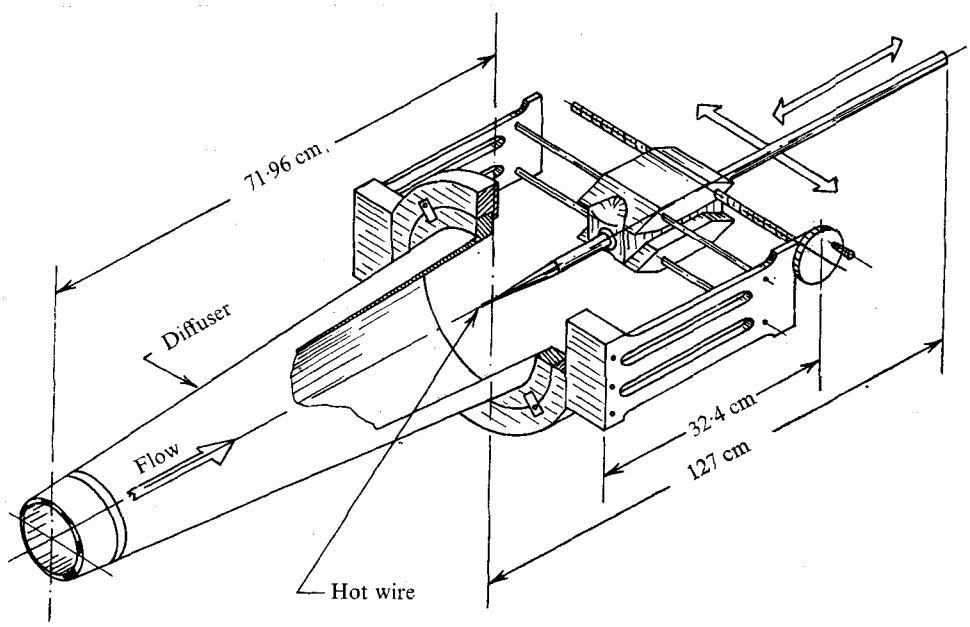

FIGURE 2. Diffuser traversing mechanism.

these were connected to a static pressure ring. A machined reinforcement ring which could be rotated to any angular position was adapted to the outlet end to support the traversing mechanism (figure 2) with a micrometer head graduated in 0·001 in. The probes were mounted on a tube entering the diffuser from the downstream end. (The size of the tube, 2·5 cm in diameter, was determined by the hot-wire probe lead connectors; a taper 22 cm long was fitted between the end of the tube and the probe support to minimize any flow blockage effect upstream of the probe.) The hot-wire holder could be rotated about its axis to align the X-probe sensors with the x_1, x_2 or x_1, x_3 planes; the line of traverse was normal to the diffuser axis.

2.2. *Measuring equipment*

Mean static and total pressures across the diffuser at each station were measured by means of round tubes with external and internal diameters of 1 mm and 0·76 mm respectively. The flow near the wall was examined for evidence of separation using flattened-tip forward- and reverse-facing Pitot tubes with external and internal tip heights of 0·45 mm and 0·15 mm respectively. The width of the tubes at the tip was 2·5 mm. The probe readings were recorded on a Betz projection manometer (discrimination 0·1 mm of water) for large pressure differences and a Hero precision micromanometer (discrimination 0·01 mm of alcohol) for small pressure differences.

Velocity fluctuations were measured with standard Disa hot-wire equipment (constant-temperature anemometers 55 D 01; linearizers 55 D 10; d.c. voltmeter 55 D 30; random signal indicators and correlators 55 A 06; and X-probe 55 A 38).

The frequency spectra were measured with a Hewlett–Packard model 3590 A

Reynolds number, $\langle U_1 \rangle D/\nu$	293000
Cross-section average velocity, $\langle U_1 \rangle$ (m/s)	45·7
Centre-line velocity, $U_{1,m}$ (m/s)	54·9
Friction velocity, U_* (m/s)	1·94
Kinematic viscosity, ν (m^2/s)	$1{\cdot}59 \times 10^{-5}$
Density, ρ (kg f s^2/m^4)	0·118

TABLE 1. Mean flow parameters at the reference station

wave analyser. The signals from the X-probes were recorded on a seven-channel Lyric TR 61-2 FM magnetic tape recording system with an upper frequency limit of 20000 Hz. The signal-to-noise ratio for the combined hot wire, anemometer, tape recorder and wave analyser system was maintained in excess of 40 db.

2.3. *Measurements*

The mean flow parameters at the reference station are given in table 1. Wall static pressure was recorded at positions upstream of the reference station and along the diffuser wall. Pressure measurements were also taken at 1 mm from the wall at stations 1–12 with (i) the flattened-tip forward-facing Pitot tube, (ii) the flattened-tip reverse-facing Pitot tube and (iii) the static pressure tube. To obtain the correlation coefficient, two random signal correlators were used as outlined in the Disa manual.† The frequency spectra were measured at station 7.

2.4. *Corrections*

The hot wire and Pitot tube were traversed to 1 mm from the wall, where the accuracy for the probe positioning was estimated at about $\pm$ 0·05 mm. Correction for the wall effect was thus assumed to be negligible and was not applied. The X-probe effective cooling velocity and the corrections for nonlinearities caused by high-intensity turbulence were assumed and applied in the form proposed by Champagne, Sleicher & Wehrmann (1967) and Champagne & Sleicher (1967) for the linearized constant-temperature operation.

The magnetic tape recorder input–output values of the r.m.s. velocity fluctuations were compared at five radial positions at station 7; the ratio varied from 1·0 to 0·97.

3. Experimental results

3.1. *Flow specification*

Mean velocity traverses taken along two perpendicular diameters at the reference station showed that the mean velocity profile was symmetric to within $\pm$ 0·4 %; at station 10 the symmetry was within $\pm$ 1 %.

At the reference station the ratio of the cross-sectional average to maximum velocity $(\langle U_1 \rangle / U_{1,m})_{\text{ref}}$, which is an indication of the degree of development of the flow, was 0·82 and 0·83 for the two flows with Re = 152000 and 293000. Nikuradse (referenced in Schlichting 1968) obtained values of $\langle U_1 \rangle / U_{1,m}$ in the

† Instruction Manual 55 A 06, Disa Elektronik A/S, Herlev, Denmark.

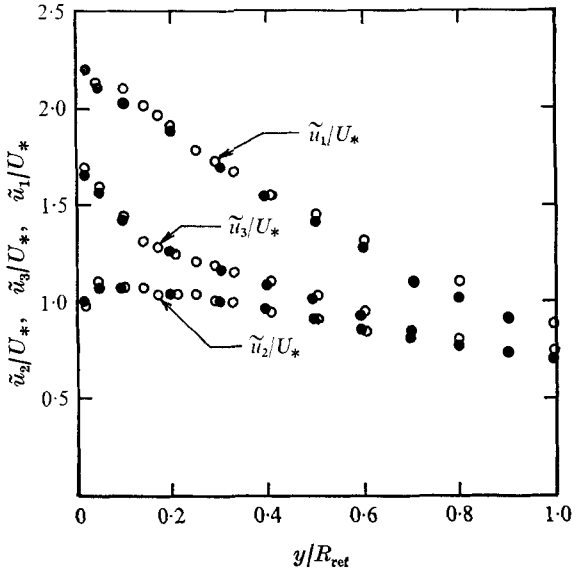

FIGURE 3. Turbulence intensities at the reference station. ●, Laufer's (1954) data, Re = 500000; ○, present data, Re = 293000.

range 0·81–0·83 for 23000 $\leqslant Re \leqslant$ 1100000 and $L/D_{\mathrm{ref}} = 120$; Lawn (1971) reported values of $\langle U_1\rangle/U_{1,m}$ in the range 0·806–0·833 for 35000 $< Re <$ 250000 and $L/D_{\mathrm{ref}} = 59$. The present values of $(\langle U_1\rangle/U_{1,m})_{\mathrm{ref}}$ therefore suggest that the flow is fully developed. A more rigorous criterion for establishing fully developed pipe flow is that the rate of change of all mean quantities (excluding pressure) with respect to the axial flow direction is zero. Experimental evidence (e.g. Laufer 1954) has shown that a value for L/D_{ref} of 50 is adequate. Here a value for L/D_{ref} of 78 is used. The distribution of the turbulence intensities (figure 3) at the reference station is shown in relation to Laufer's (1954) data to indicate the condition of the flow entering the diffuser. Here, the wall shear stress was evaluated from the wall pressure gradient upstream of the reference station.

3.2. *Mean pressure*

The mean pressure distributions along the diffuser wall as well as at 1 mm from the wall are presented in figure 4. The readings of the wall pressure, the static pressure and the reverse-facing Pitot tube pressure were practically the same; the forward-facing Pitot tube indicated correspondingly higher readings all along the diffuser wall up to the exit, thus showing that there was forward flow very close to the wall and that separation had not been reached.

3.3. *Mean velocity*

The mean axial velocities obtained from hot-wire measurements are plotted in figure 5. The decrease in the slope and magnitude of the profiles, especially near the wall, is due to the retardation of the fluid layers relative to each other caused by the rising pressure in the downstream direction. Physically, the change in

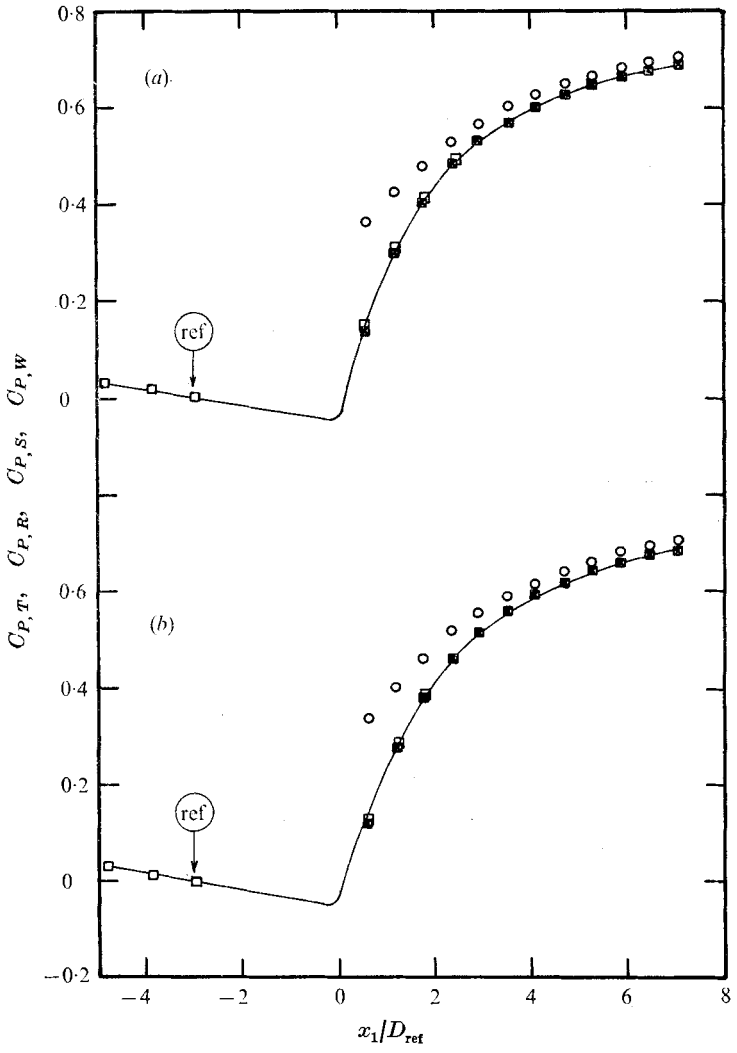

FIGURE 4. Mean pressure distribution: (*a*) $Re = 293000$; (*b*) $Re = 152000$. ○, $C_{P,T}$; △, $C_{P,R}$; □, $C_{P,W}$; ×, $C_{P,S}$. $C_{P,T} = (P_T - P_{W,\text{ref}})/\frac{1}{2}\rho \langle U_1 \rangle^2_{\text{ref}}$; R refers to the reverse-facing Pitot tube measurement; T, total; W, wall; S, static.

the diffuser cross-section in the axial direction produces a reduction in U_1 as demanded by flow continuity, and a simultaneous rise in pressure; because the radial variation of the static pressure is comparatively small, the amount by which the axial velocity is reduced would tend to be of the same order of magnitude across the diffuser, but is modified by the shear forces. The velocity profiles therefore show the biggest change of shape in regions of low velocity (near the wall). It is from stations 6–10 that the velocity profiles start exhibiting points of inflexion usually observed in boundary layers in adverse pressure gradients. The data are plotted in universal co-ordinates in figure 6(*a*). The wall shear stress was determined by extrapolating to the wall as shown in figure 6(*b*) the total

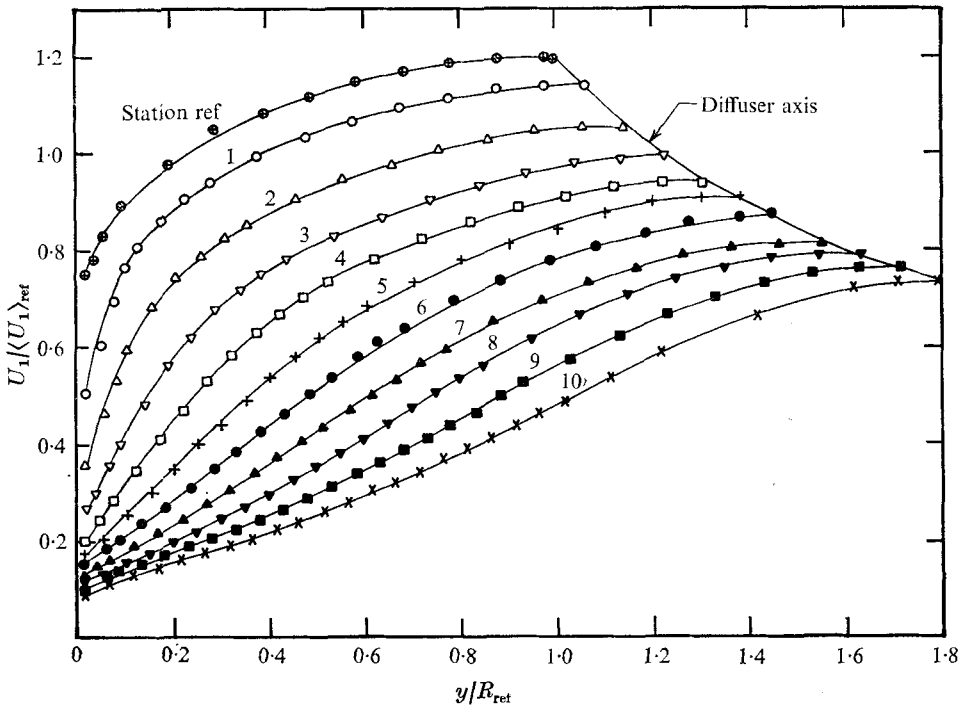

FIGURE 5. Mean velocity profiles $U_1/\langle U_1\rangle_{ref}$.

mean shear stress calculated from the sum of the viscous shear and the directly measured Reynolds stress using the equation

$$\frac{\tau}{\rho} = \nu\frac{\partial U_1}{\partial y} - \overline{u_1 u_2}. \tag{1}$$

The noteworthy feature of figure 6 (*a*) is the absence of the logarithmic region of the 'law of the wall'; a semi-logarithmic variation occurs near the axis in a region which, for fully developed pipe flow, would be associated with the velocity defect law.

The mean radial velocity distribution shown in figure 7 was evaluated from the continuity relation

$$\frac{U_2}{\langle U_1\rangle_{ref}} = -\frac{1}{r}\int_0^r \frac{\partial}{\partial x_1}\left(\frac{x_2 U_1}{\langle U_1\rangle_{ref}}\right)dx_2. \tag{2}$$

By comparing the values of $U_2/\langle U_1\rangle_{ref}$ with the values of $U_1/\langle U_1\rangle_{ref}$ in figure 5, it is seen that for $y/R_{ref} > 0{\cdot}02$ the ratio U_2/U_1 is generally less than 6 %.

3.4. *Turbulence intensities*

The distributions of the three components of the r.m.s. relative turbulence intensities are shown in figure 8. The $\tilde{u}_1$ profiles are those obtained from the average values of the X-probe readings in the x_1, x_2 and x_1, x_3 planes. At each station the $\tilde{u}_1$ component has the highest value, with $\tilde{u}_1/U_1 > \tilde{u}_3/U_1 > \tilde{u}_2/U_1$ and the degree of anisotrpoy decreasing from the wall to the diffuser axis; the $\tilde{u}_2$ component

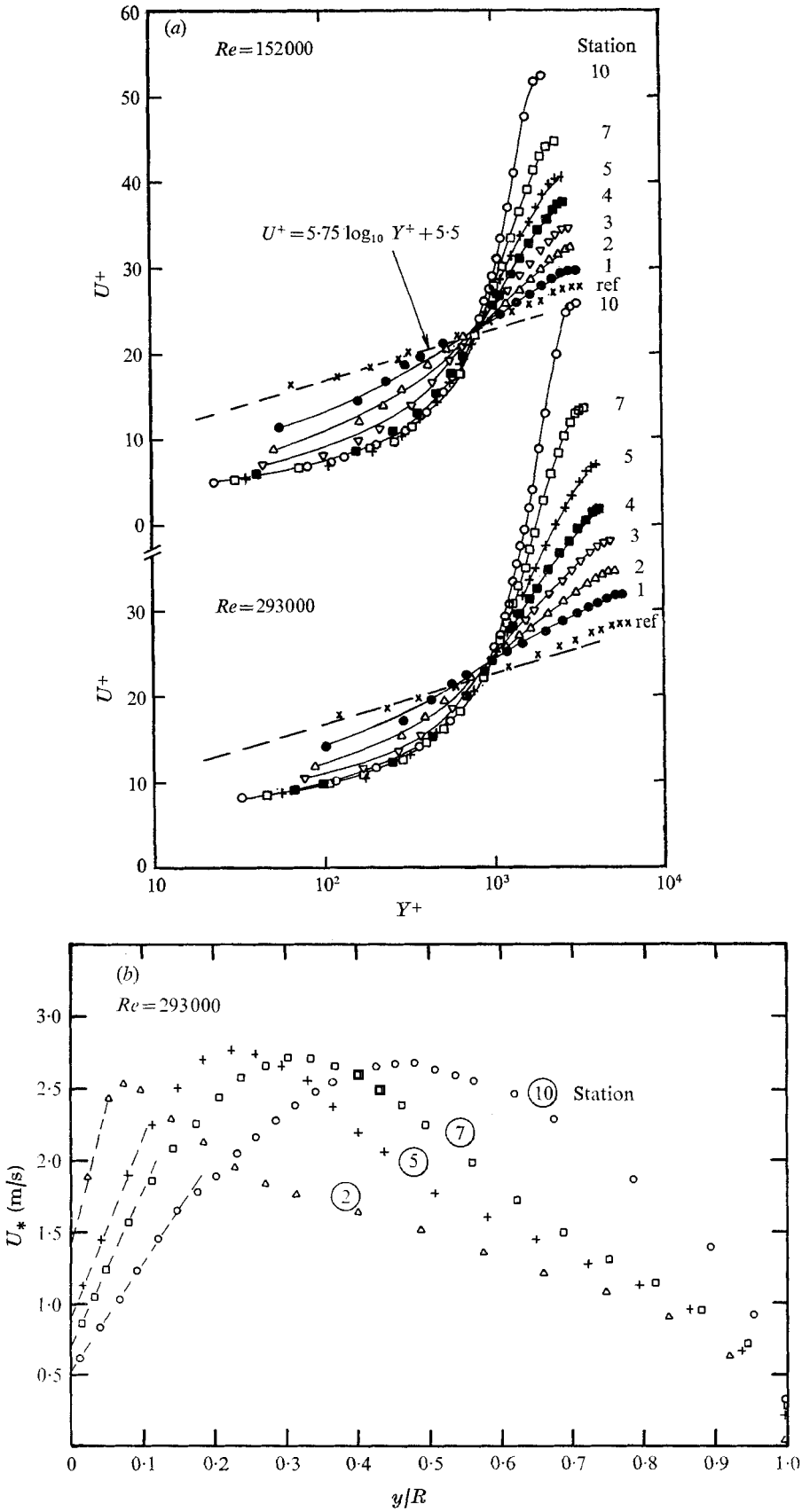

FIGURE 6. (*a*) Diffuser velocity profiles in universal co-ordinates; Re = 152000 and 293000. (*b*) Variation of the total shear stress; Re = 293000.

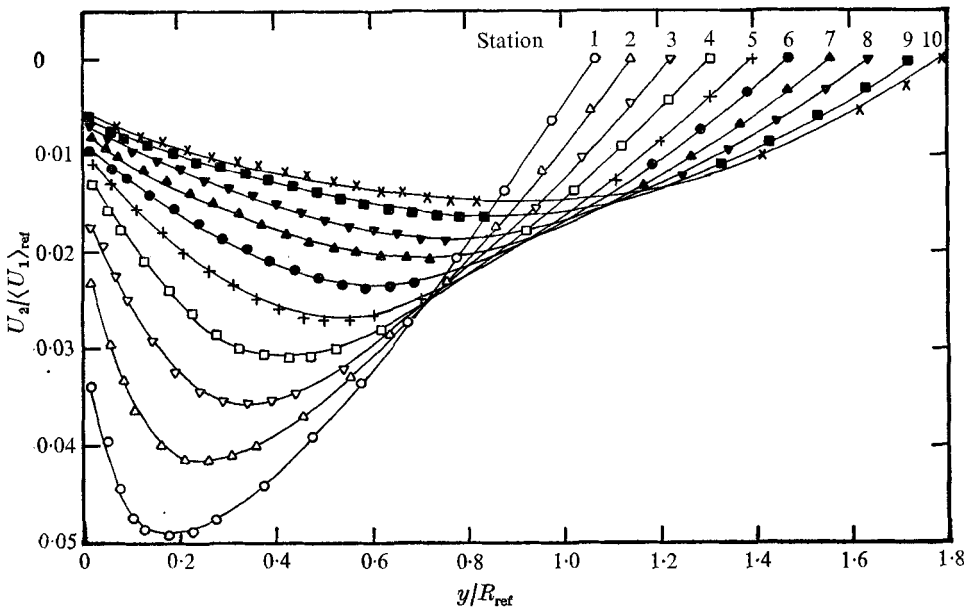

FIGURE 7. Mean velocity profiles $U_2/\langle U_1\rangle_{ref}$; $Re = 293000$.

shows a peak away from the wall; the distributions of the intensity levels are qualitatively similar to those of measurements by Klebanoff (1954) for boundary-layer flow, Laufer (1954) for fully developed pipe flow, Reutenik & Corrsin (1955) for slightly divergent channel flow, Robertson & Calehuff (1957) and Trupp *et al.* (1971) for diffuser flow.

The components of the turbulence intensity non-dimensionalized with the friction velocity (obtained by total shear stress extrapolation) are plotted in figure 9. The peak which is developed very close to the wall near the diffuser inlet moves progressively outwards in the streamwise direction; the trend is in qualitative agreement with the observations of Sandborn & Slogar (1955) in two-dimensional adverse pressure gradients.

3.5. *Correlation coefficients*

The correlation coefficient $\overline{u_1 u_2}/\tilde{u}_1\tilde{u}_2$ (figure 10) varies appreciably in the radial direction. The noteworthy features of the data are the progressive contraction of the region of constant coefficient and the development of peaks with a trend similar to those noted for the turbulence intensities $\tilde{u}_1/U_*$, $\tilde{u}_2/U_*$ and u_3/U_*. Close to the wall, the correlation coefficient exhibits an approximate linear variation with the distance from the wall and the linear range grows with downstream distance.

3.6. *'Wall turbulent layer'*

In fully developed pipe flow, the edge of the viscous sublayer approximately corresponds to the point of the maximum u_1 fluctuation. This region $y^+ \lesssim 12$ is usually of interest because the bulk of the direct viscous dissipation takes place within it; at the edge, the energy production reaches a maximum value with

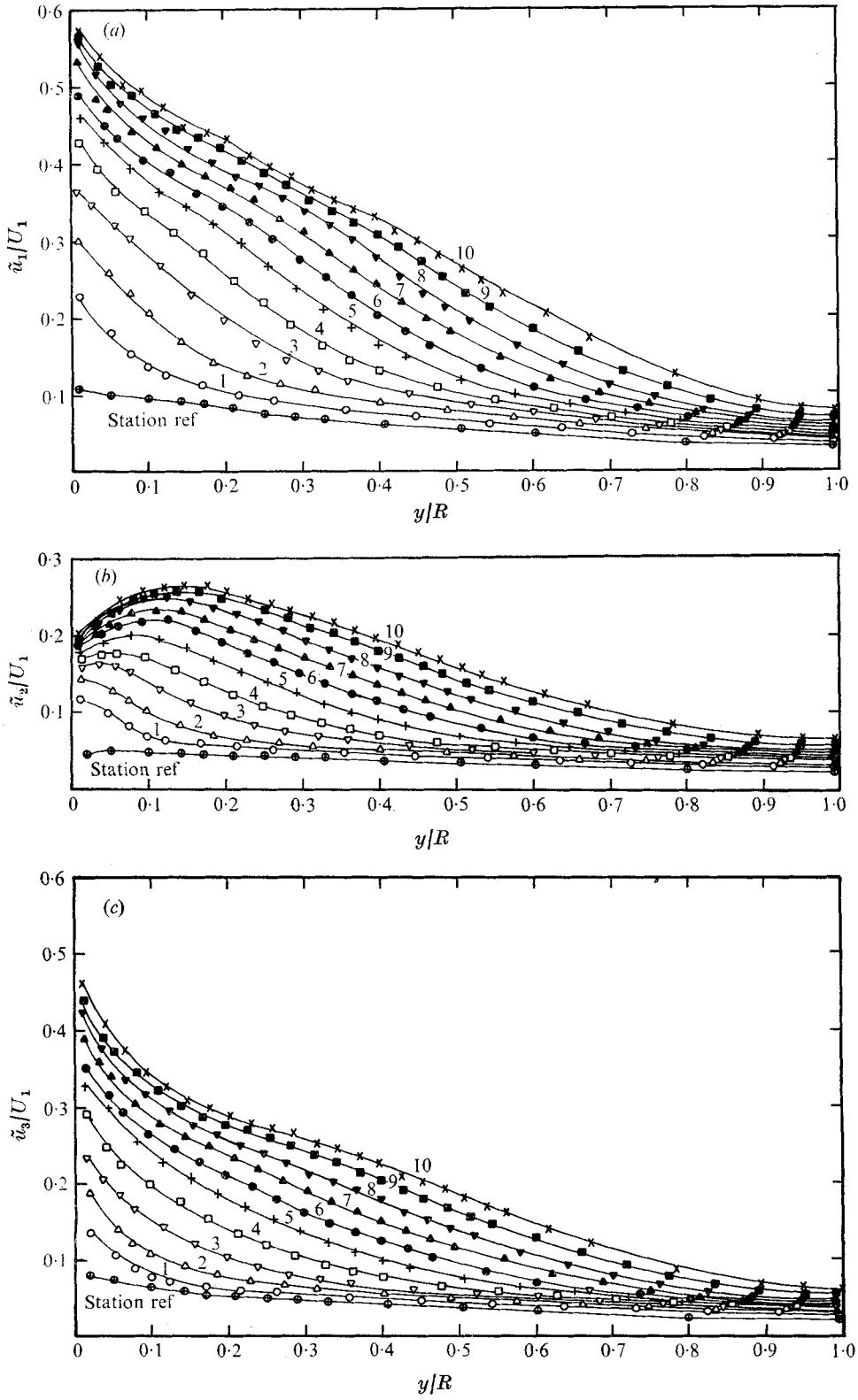

FIGURE 8. Distribution of the turbulence intensities (*a*) $\tilde{u}_1/U_1$, (*b*) $\tilde{u}_2/U_1$ and (*c*) $\tilde{u}_3/U_1$; Re = 293000.

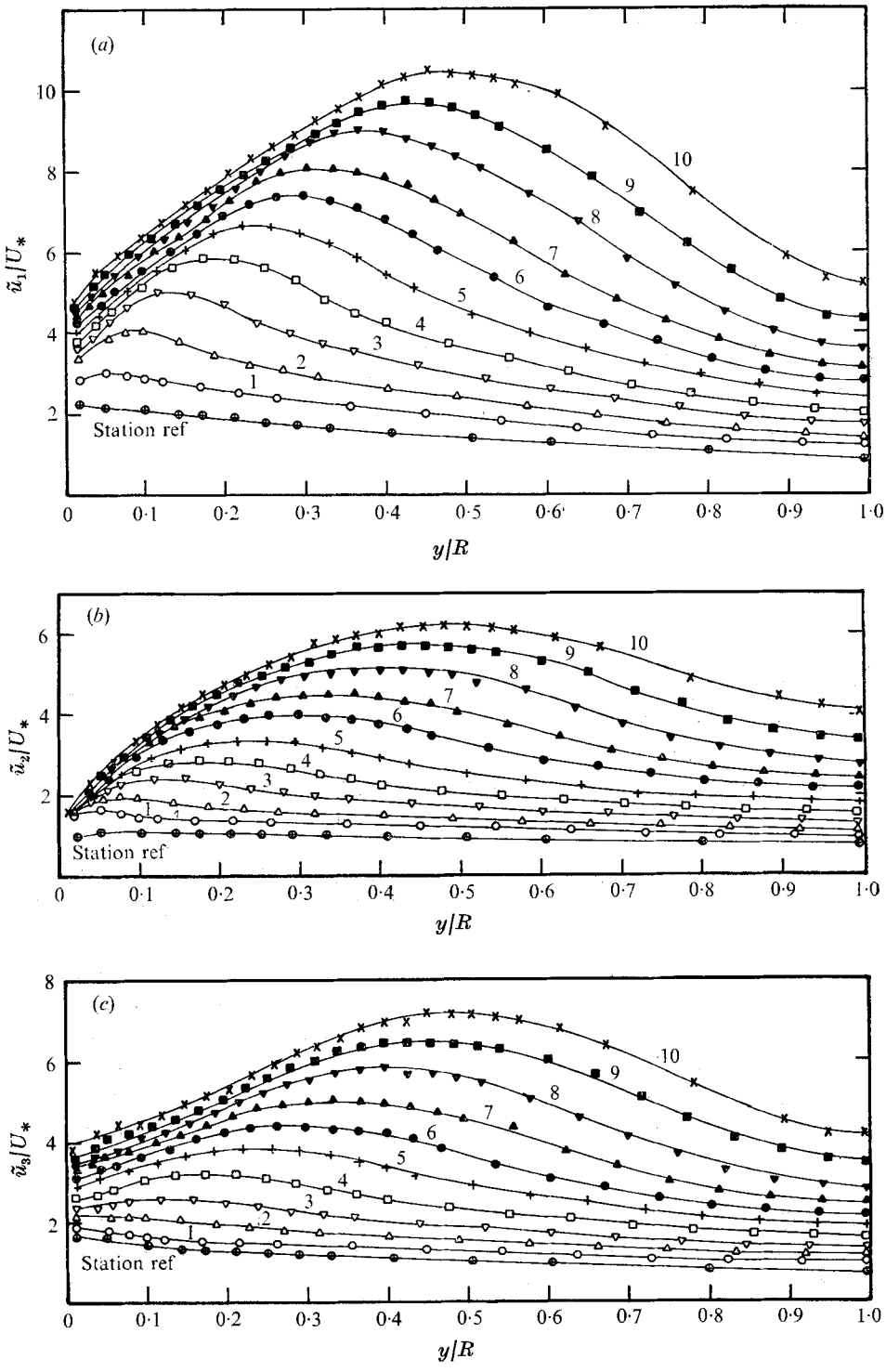

FIGURE 9. Distribution of the turbulence intensities (*a*) $\tilde{u}_1/U_*$, (*b*) $\tilde{u}_2/U_*$ and (*c*) $\tilde{u}_3/U_*$; $Re = 293\,000$.

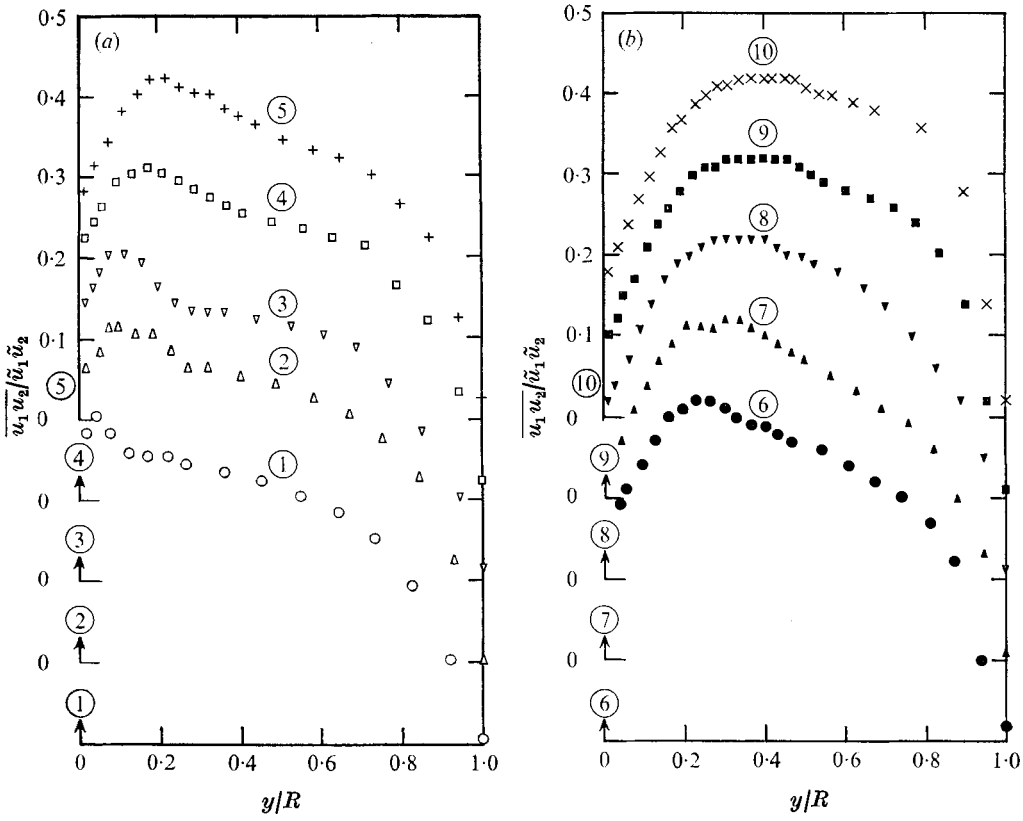

FIGURE 10. Variation of shear correlation coefficient $\overline{u_1u_2}/\tilde{u}_1\tilde{u}_2$; Re = 293000. (*a*) Stations 1–5. (*b*) Stations 6–10.

production equal to dissipation; within the layer, $\tilde{u}_1/U_*$ is linear with the distance from the wall as shown by the work of Laufer (1954) and Bakewell & Lumley (1967).

It is perhaps of interest to examine for the diffuser the flow characteristics in the layer between the wall and the point of maximum u_1-fluctuation. As in pipe flow, the energy production (figure 11) attains a maximum value approximately at the edge of the layer and the bulk of the direct viscous dissipation takes place within it. When the mean square of the streamwise velocity fluctuation $\overline{u_1^2}$ is plotted in universal co-ordinates (see figure 12) there is a linear variation in this layer; the surfaces of maximum $\overline{u_1^2}$ and $\overline{u_1u_2}$ closely coincide as shown in figure 13; at the edge of the layer the energy production rate is not in local equilibrium with the direct viscous dissipation rate as in the boundary-layer and pipe flow, rather, production is about two orders of magnitude greater than direct viscous dissipation (see figure 11), and about 60 % of the total energy production (see figure 14) takes place within the layer as compared with about 40 % for boundary layers and pipes.

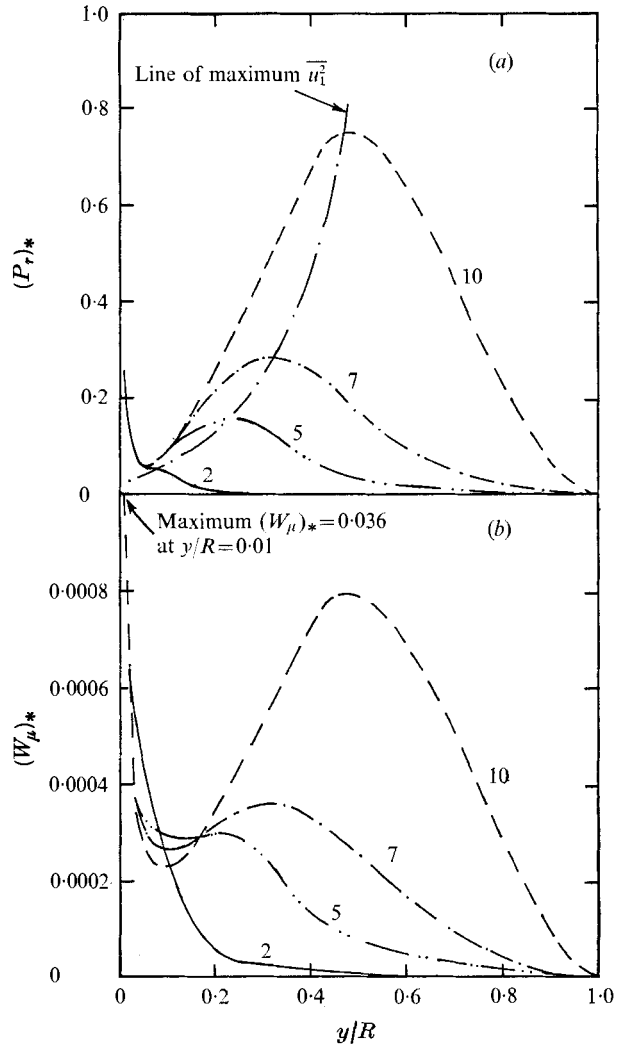

FIGURE 11. Distribution of the energy production and the direct viscous dissipation rates $Re = 293000$.

$$(a)\ (P_r)_* = \nu \frac{\overline{u_1 u_2}}{U_*^4} \frac{\partial U_1}{\partial y}; \quad (b)\ (W_\mu)_* = \frac{\nu^2}{U_*^4} \left(\frac{\partial U_1}{\partial y}\right)^2.$$

3.7. *One-dimensional spectra*

The normalized spectral density ϕ_{ij} is defined by

$$\phi_{ij}(\kappa_1 R) = F_{ij}(\kappa_1)/R\overline{u_i u_j}, \tag{3}$$

where F_{ij} is the unnormalized spectrum of $\overline{u_i u_j}$, such that

$$\int_0^\infty \frac{F_{ij}(\kappa_1)}{R} d(\kappa_1 R) = \overline{u_i u_j}.$$

The profiles of ϕ_{11} and ϕ_{22} measured at station 7 are plotted in figures 15 (*a*) and (*b*) respectively. The spectra ϕ_{11} (see figure 15 (*a*)) at varying distances from the

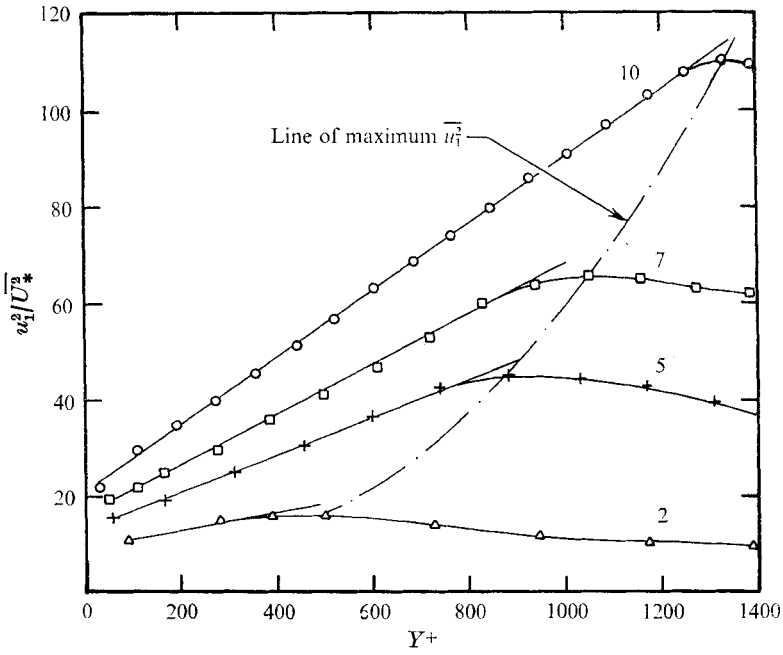

FIGURE 12. Distribution of $\overline{u_1^2}/U_*^2$ in the wall turbulent layer.

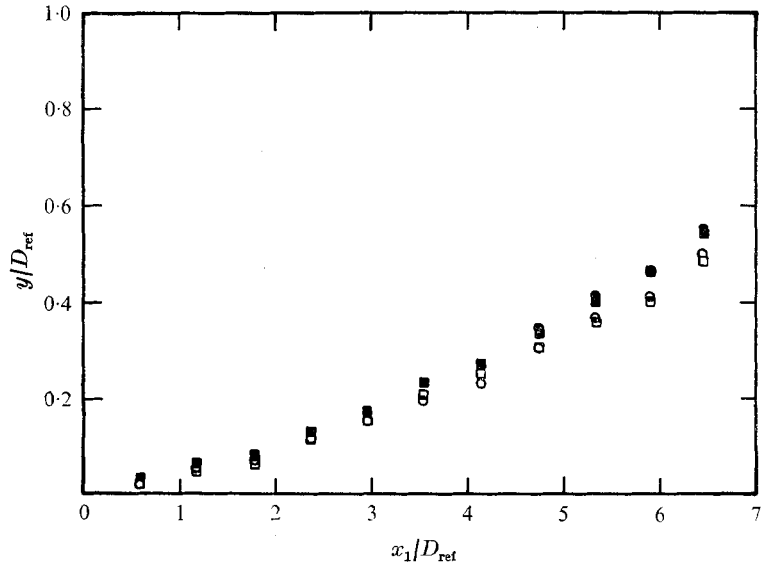

FIGURE 13. Position of maximum $\overline{u_1^2}$ and $\overline{u_1 u_2}$ as a function of the diffuser axial distance. Re = 293000: ○, $\overline{u_1^2}$; □, $\overline{u_1 u_2}$. Re = 152000: ●, $\overline{u_1^2}$; ■, $\overline{u_1 u_2}$.

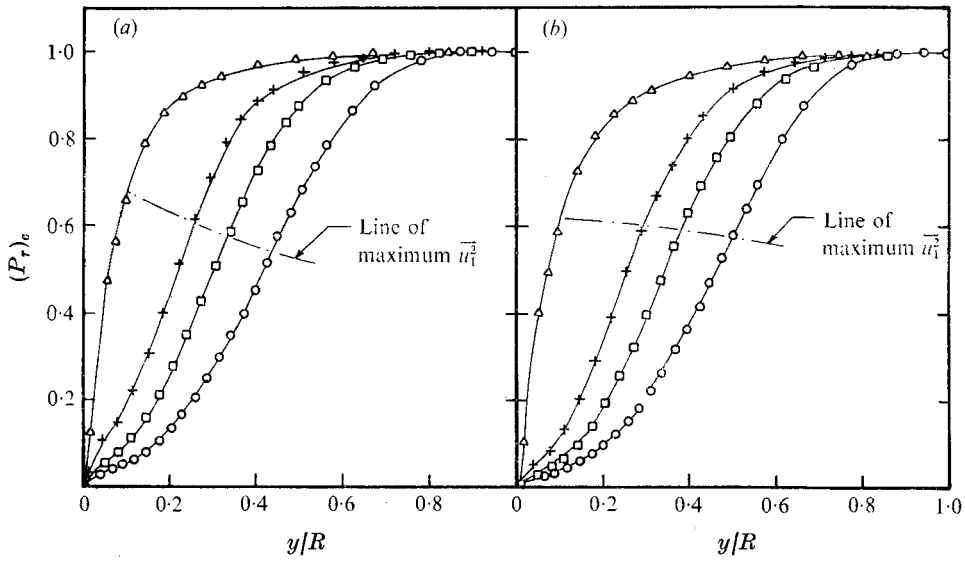

FIGURE 14. Cumulative turbulence energy production rate. (*a*) Re = 293000. (*b*) Re = 152000.

$$(P_r)_c = \frac{\int_0^{y/R} \left(1-\frac{y'}{R}\right) \overline{u_1 u_2} \frac{\partial U_1}{\partial y'} dy'}{\int_0^1 \left(1-\frac{y}{R}\right) \overline{u_1 u_2} \frac{\partial U_1}{\partial y} dy}.$$

wall for $y/R > 0{\cdot}02$ exhibit a $\kappa_1^{-\frac{5}{3}}$ dependence in the portion $9 < \kappa_1 R < 95$; the contribution to the turbulent energy in the low wavenumber range increases with distance from the wall and reaches a maximum value at about mid-radius. The difference between the profiles of the ϕ_{11} and ϕ_{22} spectra, figures 15(*a*) and (*b*) respectively, is that, in the low wavenumber range, the energy contents of the ϕ_{11} spectra are relatively greater than those of the ϕ_{22} spectra, as can be explained by the trend that $\overline{u_1^2} > \overline{u_2^2}$; also, the range of the $-\frac{5}{3}$-power law for the ϕ_{22} spectra is less than that for the ϕ_{11} spectra.

3.8. *Energy balance*

For axisymmetric flows, the equation for the turbulent kinetic energy balance may be written in the form

$$\text{(I)} + \text{(II)} + \text{(III)} + \text{(IV)} + \text{(V)} = 0, \tag{4}$$

where the terms have the following meanings.

Mean flow convection:

$$\text{(I)} = \frac{1}{2}\left[\left(\frac{U_1}{U_{1,m}}\right)\frac{\partial}{\partial \xi_1}\left(\frac{\overline{q^2}}{U_{1,m}^2}\right) + \left(\frac{U_2}{U_{1,m}}\right)\frac{\partial}{\partial \xi_2}\left(\frac{\overline{q^2}}{U_{1,m}^2}\right)\right].$$

Convective diffusion by kinetic and pressure effects:

$$\text{(II)} = \frac{1}{2\xi_2}\left\{\frac{\partial}{\partial \xi_1}\left[\xi_2 \overline{\left(\frac{u_1}{U_{1,m}}\right)\left(\frac{q^2}{U_{1,m}^2} + \frac{2p}{\rho U_{1,m}^2}\right)}\right] + \frac{\partial}{\partial \xi_2}\left[\xi_2 \overline{\left(\frac{u_2}{U_{1,m}}\right)\left(\frac{q^2}{U_{1,m}^2} + \frac{2p}{\rho U_{1,m}^2}\right)}\right]\right\}.$$

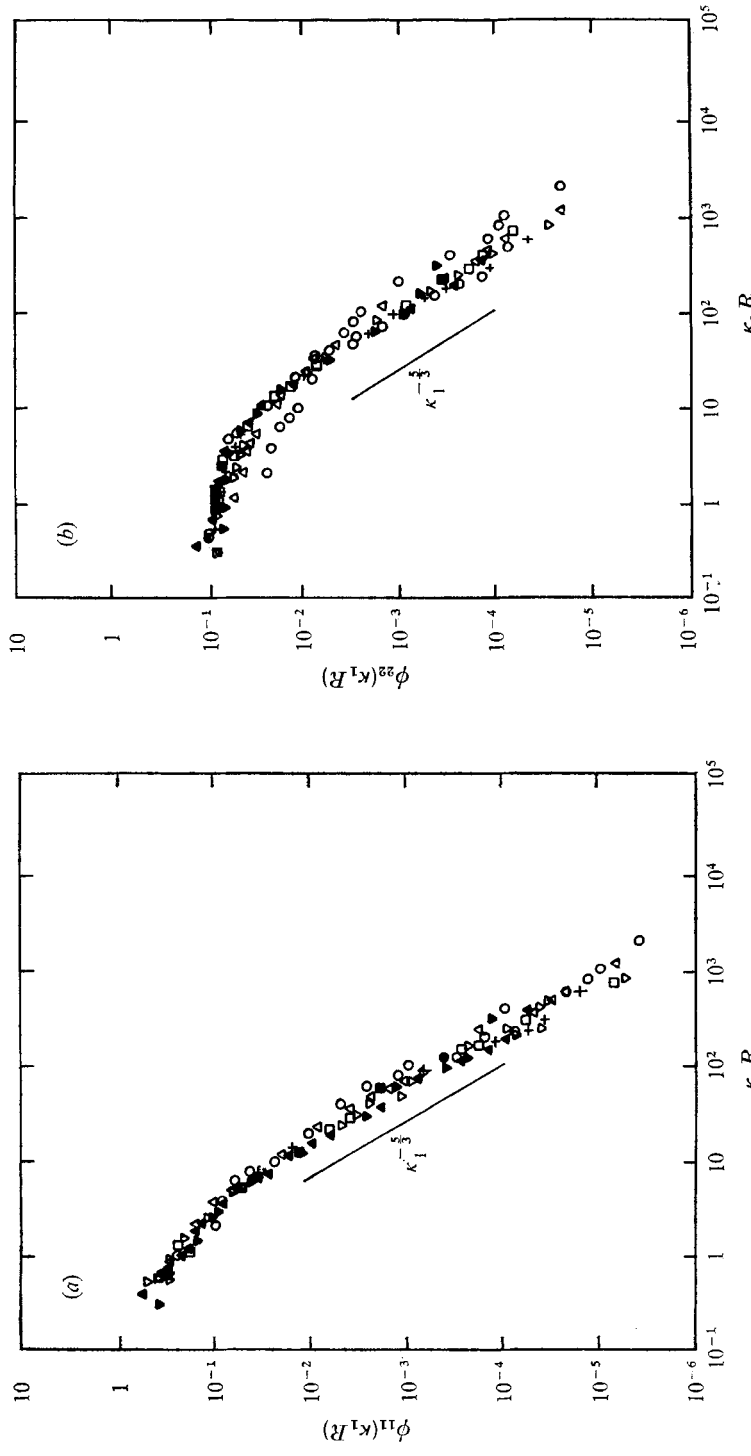

FIGURE 15. Normalized spectra of (*a*) $\overline{u_1^2}$ and (*b*) $\overline{u_2^2}$ (station 7); $Re = 293000$.

	○	△	▽	□	+	●	▲	▼	■
y/R	0·017	0·080	0·205	0·268	0·331	0·393	0·582	0·770	0·957

Production:

$$(\text{III}) = \left[\left(\frac{\overline{u_1 u_2}}{U_{1,m}^2}\right)\frac{\partial}{\partial \xi_2}\left(\frac{U_1}{U_{1,m}}\right) + \left(\frac{\overline{u_1^2}}{U_{1,m}^2} - \frac{\overline{u_2^2}}{U_{1,m}^2}\right)\frac{\partial}{\partial \xi_1}\left(\frac{U_1}{U_{1,m}}\right) + \frac{\overline{u_1 u_2}}{U_{1,m}^2}\frac{\partial}{\partial \xi_1}\left(\frac{U_2}{U_{1,m}}\right) + \frac{1}{\xi_2}\left(\frac{U_2}{U_{1,m}}\right)\left(\frac{\overline{u_3^2}}{U_{1,m}^2} - \frac{\overline{u_2^2}}{U_{1,m}^2}\right)\right].$$

Viscous work:

$$(\text{IV}) = -\left(\frac{1}{2Re_m}\left\{\frac{1}{\xi_2}\frac{\partial}{\partial \xi_2}\left[\xi_2 \frac{\partial}{\partial \xi_2}\left(\frac{\overline{q^2}}{U_{1,m}}\right)\right] + \frac{\partial^2}{\partial \xi_1^2}\left(\frac{\overline{q^2}}{U_{1,m}^2}\right)\right\} + \frac{\nu R}{U_{1,m}^3}\overline{\frac{\partial u_i}{\partial x_j}\frac{\partial u_j}{\partial x_i}}\right).$$

Dissipation:

$$(\text{V}) = R\epsilon/U_{1,m}^3.$$

Here

$$q^2 = u_i u_i, \quad \xi_1 = x_1/R, \quad \xi_2 = r/R, \quad Re_m = RU_{1,m}/\nu,$$

$$\epsilon = \nu\overline{\left(\frac{\partial u_i}{\partial x_j} + \frac{\partial u_j}{\partial x_i}\right)\frac{\partial u_i}{\partial x_j}},$$

and the normalizing quantities R and $U_{1,m}$ are taken as constants.

The distribution, at station 7, of the terms in the energy equation (4) is shown in figure 16. The mean flow convection (term I), the production (term III) and the viscous work (term IV) were evaluated directly from the data.

The dissipation (term V) was evaluated using the dissipation rate ϵ^* calculated from the $\overline{u_1^2}$ energy spectra by the method proposed by Bradshaw (1967) as

$$\epsilon^* = [F_{11}(\kappa_1)\kappa_1^{\frac{5}{3}}/0{\cdot}53]^{\frac{3}{2}}. \tag{5}$$

For comparison, a second estimate of the dissipation rate was obtained from the isotropic relationship

$$\epsilon_{\text{iso}}^* = 15\nu\overline{u_1^2}/\lambda_{u_1}^2, \tag{6}$$

where λ_{u_1} is the Taylor microscale evaluated from

$$\lambda_{u_1} = \left[\int_0^L \kappa_1^2 \phi_{11}(x_1 R)\, d(x_1 R)\right]^{-\frac{1}{2}},$$

where L is the upper limit of $(\kappa_1 R)$ reached in the measurement. The dissipation rates from equations (5) and (6) are given in table 2. At about mid-radius, the magnitudes are approximately the same; from the diffuser wall to about mid-radius, $\epsilon_{\text{iso}}^* > \epsilon^*$, while from about mid-radius to the diffuser axis, $\epsilon_{\text{iso}}^* < \epsilon^*$. The latter trend may be explained by noting the fact that higher and higher frequency components contribute to the energy spectrum as the velocity increases. Thus, more and more high frequency energy appears as the centre of the diffuser is approached. So it is quite probable that, in this region, λ_{u_1} is overestimated because of neglect of the contribution of the high frequency end of the ϕ_{11} spectrum. The comparison of ϵ_{iso}^* and ϵ^* thus provides an indication of the maximum value of the dissipation rate at station 7.

Equation (4) has been employed to determine the diffusion (term II) as the closing entry in the energy balance. The viscous work is about two orders of magnitude less than the production. The profile of the energy production shows

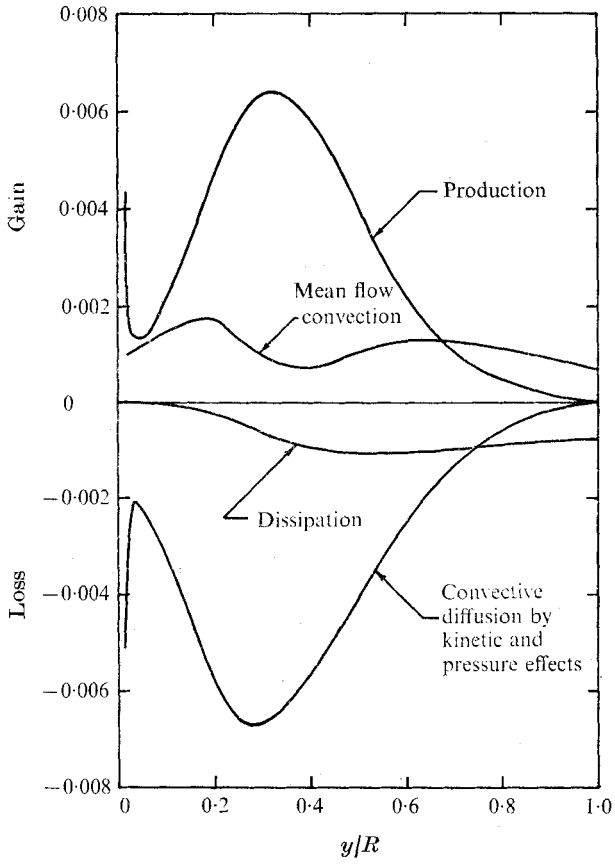

FIGURE 16. Turbulent kinetic energy balance (station 7); $Re = 293000$.

y/R	ϵ^*_{iso} (m^2/s^3)	ϵ^* (m^2/s^3)	$R\epsilon^*/U_{1,m}^3$
0·017	160·0	8·30	$0·013 \times 10^{-3}$
0·080	240·0	38·5	$0·058 \times 10^{-3}$
0·205	407·0	186·0	$0·281 \times 10^{-3}$
0·268	435·0	305·0	$0·463 \times 10^{-3}$
0·331	497·0	546·0	$0·828 \times 10^{-3}$
0·393	635·0	609·0	$0·924 \times 10^{-3}$
0·582	526·0	709·0	$1·076 \times 10^{-3}$
0·770	360·0	608·0	$0·923 \times 10^{-3}$
0·957	239·0	545·0	$0·826 \times 10^{-3}$

TABLE 2. Dissipation rate in the diffuser at station 7 for $Re = 293000$

a local minimum value near the wall ($y/R \doteq 0·03$); this trend is a result of the decrease of $\partial U_1/\partial y$ close to the wall due to the adverse pressure gradient as can be observed from figure 5 (station 7).

From the energy balance shown in figure 16, the following conclusions may be drawn.

(i) In the region $0{\cdot}8 < y/R < 1{\cdot}0$, the dissipation is mostly balanced by the mean flow convection; here, the picture is different from that for fully developed pipe flow (e.g. Laufer 1954) in that, in the latter case, the dissipation is mostly balanced by the kinetic energy diffusion, while the mean flow convection is zero.

(ii) For $0{\cdot}2 < y/R < 0{\cdot}8$, the energy production and the convective diffusion due to kinetic and pressure effects are approximately equal in magnitude while the mean flow convection, which is comparatively less than the production, is approximately equal in magnitude to the dissipation. The increased significance of the convective diffusion of turbulence due to kinetic and pressure effects in the diffuser flow is attributable to the fact that the portion

$$\frac{1}{2\xi_2}\left\{\frac{\partial}{\partial\xi_1}\left[\xi_2\overline{\left(\frac{u_1}{U_{1,m}}\right)\left(\frac{q^2}{U_{1,m}^2}+\frac{2p}{\rho U_{1,m}^2}\right)}\right]\right\}$$

of term II, equation (4), is zero in fully developed pipe flow but non-zero for the diffuser flow; the convective diffusion of turbulence may therefore be viewed here as taking place both in the streamwise and transverse directions.

(iii) For $0{\cdot}01 < y/R < 0{\cdot}2$, the rate of energy production and convection by mean motion is mostly balanced by the rate of energy convective diffusion due to kinetic and pressure effects.

The picture which emerges from the energy balance is that the magnitude of the convective diffusion of turbulence due to kinetic and pressure effects is increased in relation to that of the dissipation and is comparable with that of the production; the picture is different from those in constant-pressure boundary-layer and fully developed pipe flow, where the rate of turbulence production is comparable with the rate of turbulence dissipation.

4. Concluding remarks

An experimental study of mean and turbulent flow properties in a conical diffuser with fully developed flow at entry has been described. Data presented have included, for an entry Reynolds number of 293 000, measurements of the mean pressure, mean velocity, turbulence intensities, correlation coefficients and the one-dimensional energy spectra.

The general feature of the radial distribution of the turbulent fluctuations and the correlation coefficients is the occurrence of a peak very close to the wall near the diffuser inlet; the peak progressively shifts away from the wall with distance in the streamwise direction. The distribution of the turbulence intensity levels is qualitatively similar, but quantitatively much in excess of those in pipe flow.

The results show that the rate of turbulent energy production approximately reaches a maximum value at the edge of the wall layer extending to the point of maximum u_1-fluctuation. It is found that, within the layer, $\overline{u_1^2}$ varies linearly with distance from the wall and the linear range grows with distance in the downstream direction. The surfaces of maximum $\overline{u_1^2}$ and $\overline{u_1 u_2}$ closely coincide. At the edge of the layer, the energy production is about two orders of magnitude greater than

the direct viscous dissipation and about 60 % of the total energy production takes place in the layer.

The spectra profiles and characteristics are very similar to those reported for pipe flows; the normalized spectra of $\overline{u_1^2}$ exhibit the $\kappa_1^{-\frac{5}{3}}$ dependence for about one decade of the one-dimensional wavenumber κ_1.

From the turbulent kinetic energy balance it is found that the magnitude of the energy convective diffusion due to kinetic and pressure effects is comparable with that of the energy production.

We thank Rudy Hummel for his assistance with the electronics, and Alex Kovalcik for drawing most of the figures. The financial support of the National Research Council of Canada is gratefully acknowledged.

REFERENCES

ACKERET, J. 1967 *Gen. Motors Symp. on Internal Flow.* Elsevier.

AZAD, R. S. & HUMMEL, R. 1971 *Can. J. Phys.* **49**, 2917.

BAKEWELL, P. H. & LUMLEY, J. L. 1967 *Phys. Fluids*, **10**, 1880.

BRADSHAW, P. 1967 *Nat. Phys. Lab. Aero. Rep.* no. 1220.

CHAMPAGNE, F. H. & SLEICHER, C. A. 1967 *J. Fluid Mech.* **28**, 177.

CHAMPAGNE, F. H., SLEICHER, C. A. & WEHRMANN, O. H. 1967 *J. Fluid Mech.* **28**, 153.

COCANOWER, A. B., KLINE, S. J. & JOHNSTON, J. P. 1965 *Stanford University, Dept. Mech. Engng Rep.* PD-10.

COCKRELL, D. J. & KING, A. L. 1967 *Brit. Hydromech. Res. Ass. Rep.* TN 902.

FRASER, H. R. 1956 Ph.D. thesis, Dept. Theoretical and Applied Mech., University of Illinois.

GIBSON, A. H. 1910 *Proc. Roy. Soc.* A **83**, 366.

HARSHA, P. T. & LEE, S. C. 1970 *A.I.A.A. J.* **8**, 1508.

KLEBANOFF, P. S. 1954 *N.A.C.A. Tech. Note*, no. 3178.

KLINE, S. J., ABBOTT, D. E. & FOX, R. W. 1959 *A.S.M.E. Trans. J. Basic Engng*, **81**, 321.

LAUFER, J. 1951 *N.A.C.A. Rep.* no. 1053.

LAUFER, J. 1954 *N.A.C.A. Rep.* no. 1174.

LAWN, C. J. 1971 *J. Fluid Mech.* **48**, 477.

PATTERSON, G. N. 1938 *Aircraft Engng*, **10**, 267.

ROBERTSON, J. M. & CALEHUFF, G. L. 1957 *Proc. A.S.C.E.* **83**, HY 5, paper 1393.

RUETENIK, J. R. & CORRSIN, S. 1955 *Jahre Grenzschichtforschung*, pp. 446–459. Braunschweig: Vieweg.

SANDBORN, V. A. & SLOGAR, R. J. 1955 *N.A.C.A. Tech. Note*, no. 3264.

SCHLICHTING, H. 1968 *Boundary-Layer Theory*, 6th edn. McGraw-Hill.

SOVRAN, G. & KLOMP, E. D. 1967 *Gen. Motors Symp. on Internal Flow.* Elsevier.

SPRENGER, H. 1959 *Mitt. Inst. Aero. Zurich*, no. 27. (See also 1962 *Brit. Min. Aviation Rep.* TIL/T. 5134.)

TRUPP, A. C. AZAD, R. S., WILSON, N. W. & OKWUOBI, P. A. C. 1971 *University of Salford Symposium on Internal Flows*, paper 9.

VENTURI, G. B. 1797 *Nicholson's Journal of Natural Philosophy*, vol. 3. London, 1802.